Molecular Dynamics of 1-Palmitoyl-2-oleoylphosphatidylcholine Membranes Containing Transmembrane α-Helical Peptides with Alternating Leucine and Alanine Residues[†]

Witold K. Subczynski,*,[‡] Marta Pasenkiewicz-Gierula,[§] Ronald N. McElhaney,[||] James S. Hyde,[‡] and Akihiro Kusumi[⊥]

Biophysics Research Institute, Medical College of Wisconsin, Milwaukee, Wisconsin 53226, Biophysics Department, Institute of Molecular Biology, Jagiellonian University, Krakow, Poland, Department of Biochemistry, University of Alberta, Edmonton, Alberta, Canada T6G 2H7, Department of Biological Science, Nagoya University, Nagoya 464-8602, Japan, and Kusumi Membrane Organizer Project, Exploratory Research on Advanced Technology Organization, JST, Kumazaki Building, 5-11-33 Chiyoda, Nagoya 464-0012, Japan

ABSTRACT: The effects of the transmembrane α-helical peptide Ac-K$_2$(LA)$_{12}$K$_2$-amide [(LA)$_{12}$] on the molecular organization and dynamics of 1-palmitoyl-2-oleoylphosphatidylcholine (POPC) membranes were investigated using conventional and saturation−recovery EPR observations of phosphatidylcholine spin labels, and the results were compared with our earlier, similar study of Ac-K$_2$L$_{24}$K$_2$-amide (L$_{24}$) [Subczynski, W. K., Lewis, R. N. A. H., McElhaney, R. N., Hodges, R. S., Hyde, J. S., and Kusumi, A. (1998) *Biochemistry 37*, 3156−3164]. At peptide-to-POPC ratios between 1/10 and 1/40, both methods (covering a time scale of 100 ps−10 μs) detect the presence of a single homogeneous membrane environment for both peptides, suggesting that these peptides are both well dispersed and that POPC is exchanging rapidly between the boundary and the bulk domains. The local diffusion−solubility product of oxygen molecules (oxygen transport parameter) in the membrane, studied by saturation−recovery EPR, decreases by a factor of about 2 by including 10 mol % (LA)$_{12}$ whereas incorporating L$_{24}$ has practically no effect. (LA)$_{12}$ increases the alkyl chain order of POPC more than L$_{24}$. L$_{24}$ increases hydrophobicity (decreases the degree of water penetration into the hydrophobic region of the membrane) more than does (LA)$_{12}$. We ascribe the much stronger effects of (LA)$_{12}$ on membrane order and dynamics to the increased roughness of its hydrophobic surface and also to the increased motional freedom of its leucine side chains. In L$_{24}$, the leucine side chains are packed tightly, giving a smooth hydrophobic surface. In (LA)$_{12}$, they are separated by the small methyl groups of the alanine side chains, giving them additional motional freedom and the ability to protrude between the phospholipid hydrocarbon chains. The frequency of *gauche−trans* isomerization of hydrocarbon chains and concentration of vacant pockets (voids) in the lipid bilayer are thus reduced, which decreases oxygen transport. This explanation was confirmed by calculating the orientational order of leucine side chains in (LA)$_{12}$ and L$_{24}$ from molecular dynamics simulation studies.

Proteins do not float freely in a sea of excess lipids in the cellular membrane, and the nonrandom distribution of proteins, protein-rich domains, and protein oligomeric structures play important functional roles (*1−8*). Many functions of the plasma membrane are directly linked to the formation of specific protein complexes and protein-rich domains, such as signaling and protein sorting complexes (*9−16*), cell−cell adhesion structures (*16−19*), and caveolae (*20−22*). A critical issue in understanding membrane domains is the realization that these domains are not static structures. First,

the domains may form and disintegrate continually, with lifetimes ranging from nanoseconds to seconds, and up to hours (*17, 23−25*). Second, even in long-lived domains, the constituent molecules may be rapidly exchanging. Some molecules go out while other molecules come in, as in micelles in which constituent molecules move in and out continuously (*5, 26*).

In the present research, we are concerned with the basic interaction between formation and molecular organization of membrane oligomers and protein-rich domains within the membrane. We paid special attention to three types of organizations of membrane components: protein-rich domains, protein association, and specific lipid domains. Investigation of the first and the second types of organization involves the use of model peptides to better understand molecular organization in protein-rich domains and molecular interactions that lead to formation of protein-rich domains. In those studies, we used various artificial transmembrane α-helical peptides. We were particularly concerned with how

* Corresponding author. Tel: 414-456-4038. Fax: 414-456-6512. E-mail: subczyn@mcw.edu.
‡ Medical College of Wisconsin.
§ Jagiellonian University.
|| University of Alberta.
⊥ Nagoya University and Exploratory Research on Advanced Technology Organization.

α-helical peptides are packed and organized in the membrane at high peptide concentrations.

A number of researchers have designed and synthesized peptide models of specific regions of natural membrane proteins and have studied their interactions with model lipid membranes of different composition (*27*, *28*). Particularly, the synthetic peptide Ac-$K_2GL_{24}K_2$-amide (P_{24})[1] and its analogues have been successfully utilized as a model of the hydrophobic transmembrane α-helical segments of integral membrane proteins (*28*, *29*). Both CD (*29*) and Fourier transform infrared (FTIR) (*30−32*) spectroscopic studies of P_{24} have shown that it adopts a very stable α-helical conformation both in solution and in lipid bilayers, and X-ray diffraction (*33*), fluorescence quenching (*34*), and FTIR spectroscopic (*30−31*) studies have confirmed that P_{24} and its analogues assume a transbilayer orientation when reconstituted with various PCs. Differential scanning calorimetry DSC (*29*, *31*, *35−37*) and ^2H nuclear magnetic resonance (NMR) spectroscopic (*29*, *36*, *37*) studies have shown that P_{24} broadens the gel/liquid-crystalline phase transition and reduces its enthalpy. The phase transition temperature is shifted either upward or downward, depending on the degree of mismatch between the hydrophobic length of the peptide and the hydrophobic thickness of the PC lipid bilayers (*31*).

We have previously investigated the molecular organization and dynamics of phospholipids model membranes containing the α-helical transmembrane peptides Ac-$K_2L_{24}K_2$-amide (L_{24}) (*38*) and Ac-$K_2A_{24}K_2$-amide (A_{24}) (*39*) in the picosecond to microsecond regime using spin labeling techniques. In particular, we studied (1) the hydrocarbon chain order in the 100 ns time regime, (2) the effective reorientation time of the hydrocarbon chains in the time regime of 100 ps and 10 ns, (3) the hydrophobicity profiles across the membrane, and (4) the local diffusion−solubility characteristics of oxygen in the membrane, which are sensitive to the molecular dynamics up to several microseconds. Presently, we extend our investigation to another peptide from the same class of peptides that possesses a significant roughness of the hydrophobic surface, Ac-$K_2(LA)_{12}K_2$-amide [$(LA)_{12}$]. In this peptide, the polyleucine core of L_{24} or the polyalanine core of A_{24} was replaced by alternating leucine and alanine residues, respectively. Replacement of half of the leucine residues by smaller and less hydrophobic alanine residues should affect its interaction with the lipid bilayer.

All peptides form α-helices in methanol and exist as a membrane α-helix when incorporated into phospholipids in the absence of water. When water is added, both L_{24} and $(LA)_{12}$ form stable transmembrane associations with the lipid bilayer (*40*, *41*). A_{24}, however, partitions strongly into the aqueous phase, where it exists primarily in a non-α-helical conformation and interacts only weakly with the lipid bilayer due to the insufficient hydrophobicity of the polyalanine core

(*39*). Conventional EPR spectra, as well as saturation−recovery curves measured in both the presence and the absence of molecular oxygen, showed that, in the case of L_{24}, phosphatidylcholine spin labels (*n*-PCs) detect the existence of a single homogeneous environment. This result indicates that the peptides as well as the phospholipids in 1-palmitoyl-2-oleoylphosphatidylcholine (POPC)−L_{24} membranes are likely to be undergoing fast translational diffusion up to 10 mol % peptide and that the exchange rates of lipids among the bulk, boundary, and L_{24} cluster regions are fast. Molecular dynamics simulations indicate that, in the liquid-crystalline phase, 10−12 molecules of phosphatidylcholine are required to surround a transmembrane α-helical peptide (*42*). Thus, L_{24} must form L_{24}-rich regions at 10 mol %, but the regions must be forming and dispersing rapidly (in a time scale shorter than 0.1 μs). This conforms to the conventional EPR spin label time scale and the electron spin−lattice relaxation time scale in the presence of molecular oxygen. Although this does not exclude the possibility of formation of stable small oligomers of L_{24}, it is unlikely, since L_{24} lacks the features to favor formation of small stable oligomers. These results have led us to inquire why L_{24} does not form larger aggregates with lifetimes longer than 0.1 μs. High peptide−POPC miscibility may be due to the four lysine groups, which place two positive charges on each side of the membrane in the peptide. These repulsive charges may be responsible for preventing aggregation of L_{24}. Another possibility is that L_{24} has a rather smooth surface and its presence only perturbs the lipid like hard cylinders placed in a lipid bilayer. Mixing entropy thus wins over the interaction free energy between L_{24} and POPC.

In the present study, we show that the effect of $(LA)_{12}$ on POPC membrane dynamics and organization is different from that of L_{24}, despite the similar presence of dilysine terminae. The differences indicated by conventional EPR spectroscopy are moderate. However, the effect of $(LA)_{12}$ on oxygen transport[2] within the lipid bilayer is significantly greater compared with the effect of L_{24}. We believe these differences are the result of differing organizations of the hydrophobic peptide surfaces in L_{24} and $(LA)_{12}$. The former can be approximated by a hard surface smooth cylinder because of the tight packing of the leucine side chains. The latter resembles a cylinder with a brush-like surface, because leucine side chains are separated by the small methyl groups of alanines. This gives $(LA)_{12}$ the capability for stronger interaction with the phospholipid hydrocarbon chains. The leucine side chains can penetrate between the phospholipid hydrocarbon chains, decreasing the frequency of *gauche−trans* isomerization of these chains and reducing the concentration of voids in the lipid bilayer, which in turn decreases oxygen transport.

MATERIALS AND METHODS

Materials. The peptide Ac-$K_2(LA)_{12}K_2$-amide [$(LA)_{12}$] was synthesized by the Protein/Nucleic Acid Shared Facility (Medical College of Wisconsin, Milwaukee). 1-

---

[1] Abbreviations: POPC, 1-palmitoyl-2-oleoylphosphatidylcholine; P_{24}, Ac-$K_2GL_{24}K_2$-amide; L_{24}, Ac-$K_2L_{24}K_2$-amide; A_{24}, Ac-$K_2A_{24}K_2$-amide; $(LA)_{12}$, Ac-$K_2(LA)_{12}K_2$-amide; *n*-PC, 1-palmitoyl-2-(*n*-doxyl-stearoyl)-L-α-phosphatidylcholine, where $n = 5, 7, 10, 12$, and 16; TEMPO-PC, 1-palmitoyl-2-oleoyl-*sn*-glycero-3-phospho(2,2,6,6-tetra-methylpiperidine-1-oxyl)choline; T_1, spin−lattice relaxation time; PC, phosphatidylcholine; SLOT domain, slow oxygen transport domain; DSC, differential scanning calorimetry; FTIR, Fourier transform infrared; NMR, nuclear magnetic resonance.

[2] In the present paper, the word "transport" is used in its basic physical sense, indicating the product of the (local) translational diffusion coefficient and the (local) concentration of oxygen in the membrane. Active transport across the membrane is not the subject of this paper.

Palmitoyl-2-(*n*-doxylstearoyl)-L-α-phosphatidylcholines (*n*-PC, where *n* = 5, 7, 10, 12, and 16), 1-palmitoyl-2-oleoyl-*sn*-glycero-3-phospho(2,2,6,6-tetramethylpiperidine-1-oxyl)-choline (TEMPO-PC), and POPC were obtained from Avanti Polar Lipids, Inc. (Alabaster, AL).

Preparation of POPC−(LA)₁₂ Membranes. The membranes used in this work were multilamellar dispersions of POPC containing 1 mol % *n*-PC or TEMPO-PC and various amounts of $(LA)_{12}$ from 0 to 10 mol %. Briefly, these membranes were prepared by the following method (*38, 39*): Chloroform solutions of POPC [$(0.3-1.0) \times 10^{-5}$ mol] and *n*-PC or TEMPO-PC and a methanol solution of $(LA)_{12}$ were mixed to attain the desired lipid-to-peptide ratio, the solvent was evaporated with a stream of nitrogen gas, and then the lipid film on the bottom of the test tube was thoroughly dried under reduced pressure (about 0.1 mmHg) for 12 h. A buffer solution (0.2 mL of 10 mM PIPES and 150 mM NaCl, pH 7.0) was added to the dried lipids at 40 °C and vortexed vigorously.

Conventional EPR. The POPC or POPC−(LA)₁₂ membranes were centrifuged briefly, and the loose pellet (about 20% lipid, w/w) was used for the EPR measurements. For conventional EPR measurements, the sample was placed in a 0.9 mm i.d. gas-permeable TPX capillary, and the capillary was placed inside the EPR dewar insert. It was then equilibrated with nitrogen gas used for temperature control (*43*). The sample was thoroughly deoxygenated at a temperature well above the phase transition temperature of the lipid bilayer. A Varian E-109 X-band spectrometer with Varian temperature control accessories and E-231 Varian multipurpose cavity (rectangular TE_{102} mode) were used. The temperature was monitored using a copper−constantan thermocouple that was placed in the sample just above the active volume of the cavity. A modulation amplitude of 0.5−1.0 G and an incident microwave power of 1.0 mW were used. EPR spectra were recorded for the temperature range 10−55 °C. To measure the hydrophobicity profiles across the membrane, the hyperfine interactions of the nitroxide were used; the sample was frozen (−165 °C), and the EPR spectra were recorded (*44*).

Saturation Recovery EPR. The T_1s of the spin labels were determined by analyzing the saturation−recovery signal of the central line obtained by short-pulse saturation−recovery EPR at X-band (*26, 45−48*). The saturation−recovery spectrometer was described previously (*23, 45, 46*). For saturation−recovery measurements, the sample was placed in a capillary (i.d. = 0.5 mm) made of a gas-permeable polymer, TPX (*49*). A relatively low level of observing power (8 μW, with the loop-gap resonator delivering an H_1 field of 3.6×10^{-5} G) was used for all experiments to avoid microwave power saturation (which induces artificial shortening of the apparent T_1). Typically, accumulations of the decay signals were carried out with 2048 data points on each decay. For measurements of the oxygen transport parameter, the concentration of oxygen in the sample was controlled by equilibration with the same gas that was used for the temperature control, i.e., a controlled mixture of nitrogen and dry air adjusted with flowmeters (Matheson Gas Products, Model 7631H-604) (*43, 49*).

To monitor the local diffusion−solubility characteristics of oxygen molecules in the membrane, the bimolecular collision rate between oxygen (a fast relaxing species) and

the nitroxide spin label (a slow relaxing species) placed at specific locations in the membrane was evaluated in terms of an oxygen transport parameter [$W(x)$]. $W(x)$ was defined as

$$W(x) = T_1^{-1}(\text{air}, x) - T_1^{-1}(N_2, x) \quad (1)$$

where the T_1s are the spin−lattice relaxation times of the nitroxide in samples equilibrated with atmospheric air and nitrogen, respectively (*43, 48, 50*). $W(x)$ is proportional to the product of the local translational diffusion coefficient $D(x)$ and the local concentration $C(x)$ of oxygen [thus $W(x)$ is called a "transport" parameter] at a "depth" x in a lipid bilayer that is equilibrated in the atmospheric air:

$$W(x) = AD(x)C(x) \qquad A = 8\pi pr_0 \quad (2)$$

where r_0 (about 4.5 Å) is the interaction distance between oxygen and the nitroxide radical spin label (*51, 52*) and p is the probability that an observable event occurs when a collision does occur[3] and is very close to one (*49, 53, 54*).

Molecular Dynamics Simulations. Molecular dynamics simulations of the peptides were carried out for 1 ns each, in a vacuum at 37 °C, using AMBER 4.0 (*55*). The all-atom model and AMBER force field were used. Restraints of a flat bottom harmonic potential (*56*) were imposed on the phi and psi torsion angles to preserve the α-helical structure of the peptides during simulation.

The molecular order parameter, S_{mol}, was adopted from Hubbell and McConnell (*57*)

$$S_{mol} = (1/2)\langle 3\cos^2\theta_n - 1 \rangle \quad (3)$$

where θ_n is an instantaneous angle between the $C_\alpha - C_\gamma$ vector (linking C_α and C_γ carbon atoms of the side chain of the *n*th leucine) in the dynamic structure (time > 0 ps) and the $C_\alpha - C_\gamma$ vector in the initial energy-minimized structure (time = 0 ps) of the peptide. The brackets in eq 3 denote averaging over four time frames at 970, 980, 990, and 1000 ps of the simulation time. A negative value of S_{mol} indicates that the angle between the vectors is between 54.8° and 90°.

RESULTS AND DISCUSSION

Saturation Recovery Measurements. All measurements of T_1 were made on the central line of the EPR spectra between 10 and 45 °C. Figure 1 shows typical saturation−recovery curves for 16-PC in POPC and POPC−(LA)₁₂ membranes at 20 °C in the presence and absence of oxygen. The recovery curves were fitted by single, double, and triple exponentials and compared. The results indicated that, for all of the recovery curves obtained in this work, no substantial improvement in the fitting was observed when the number of exponentials was increased from one, suggesting that these recovery curves can be analyzed as single exponentials. The decay time constants were determined within an accuracy of ±3%.

Saturation−recovery measurements were carried out systematically as a function of the partial pressure of oxygen in the equilibrating gas mixture, the mole percent of peptide

---

[3] *A* is remarkably independent of the hydrophobicity and viscosity of the solvent and of the spin label species (*53, 54*).
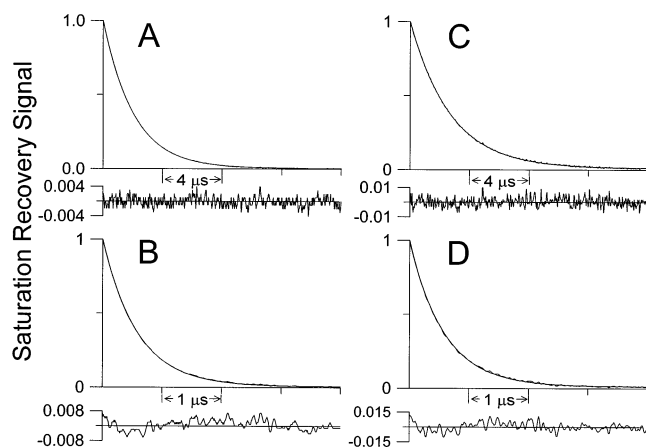
FIGURE 1: Representative saturation−recovery signals and fitted curves of 16-PC in POPC membranes in the absence (A, B) and the presence (C, D) of 10 mol % $(LA)_{12}$ at 20 °C. (B) and (D) were obtained for samples equilibrated with a gas mixture of 50% air and 50% nitrogen at 20 °C. (A) and (C) were obtained for samples equilibrated with 100% nitrogen gas. The solid lines indicate the fit to single-exponential curves with recovery times of 2.03 μs (A), 0.58 μs (B), 2.71 μs (C), and 0.92 μs (D). The difference between the experimental data and the fitted curve is shown in the lower part of each recovery curve.

Table 1: Electron Spin−Lattice Relaxation Times (T_1 in μs) for *n*-PC in POPC Membranes Containing 0 or 10 mol % $(LA)_{12}$ at Different Temperatures

temp (°C)	$(LA)_{12}$ (mol %)	T_1 (μs)					
		T-PC	5-PC	7-PC	10-PC	12-PC	16-PC
10	0	4.10	7.12	6.17	5.63	4.85	2.60
	10	4.49	8.26	7.70	6.63	6.20	3.28
20	0	3.39	5.66	4.90	4.57	4.05	2.03
	10	3.61	6.72	6.20	5.47	5.18	2.71
35	0	2.29	4.11	3.65	3.26	3.03	1.45
	10	2.54	4.88	4.45	3.88	3.76	1.91
45	0	1.90	3.37	3.00	2.76	2.57	1.27
	10	2.05	4.01	3.65	3.30	3.19	1.62

in the lipid bilayer, and the location of spin labels in the membrane, with the temperature in the range of 10−45 °C. Previously, we found that the presence of two recovery constants, i.e., the presence of two membrane environments, can be found more readily in the presence of oxygen (*26, 58*), but we always found single-exponential recovery in the present experiments. This indicates the presence of a single homogeneous membrane when averaged over 0.16 μs (the shortest recovery time observed here) at a peptide-to-POPC ratio between 1/10 and 1/40 and that, in these membranes, the rates of lipid exchange among the bulk, boundary, and peptide-rich regions are greater than the T_1 relaxation rate (greater than 6×10^6 s^{-1}; see ref *38* for more detail).

Effects of $(LA)_{12}$ on T_1 in the Absence of Molecular Oxygen. The T_1 data are summarized in Table 1. In the absence of molecular oxygen, incorporation of 10 mol % $(LA)_{12}$ increases the T_1 of all spin labels, probably due to the decrease in rotational motion of the nitroxide group in the POPC membrane (*59−61*).

Saturation−Recovery Measurements of the Oxygen Transport Parameter. In Figure 2, T_1^{-1} values for 5-, 10-, and 16-PC in POPC membranes with or without 10 mol % $(LA)_{12}$ at 20 °C are shown as a function of oxygen concentration (in percent air) in the equilibrating gas mixture. All plots of T_1^{-1} for these membranes show a linear dependence on the
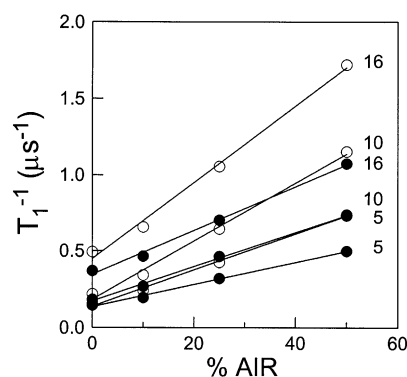

FIGURE 2: T_1^{-1} for 5-, 10-, and 16-PC in POPC (○) and POPC−$(LA)_{12}$ (10 mol %) membranes (●) at 20 °C plotted as percent air (v/v) in the equilibrating gas mixture.

oxygen concentration between 0 and 50% air for a temperature region between 10 and 45 °C for all spin labels. The oxygen transport parameter, $W(x)$, was obtained from the slope of the linear plot in Figure 2 (three decay measurements for each point in the plot), with an accuracy better than ±10% (see eq 1).

$W(x)$ values for POPC and POPC−$(LA)_{12}$ membranes are displayed in Figure 3. The presence of $(LA)_{12}$ decreases $W(x)$ at all positions in the POPC bilayer and at all temperatures.

Since the overall oxygen concentration in the liquid-crystalline phase membrane is practically independent of temperature above the phase transition temperature (*62, 63*) and the shape of the membrane profiles of $W(x)$ is practically independent of temperature in the liquid-crystalline phase, the temperature dependence of $W(x)$ can be attributed to the diffusion rate of molecular oxygen in the membrane. Since the oxygen transport parameters plotted in Figure 3 show linear dependence on the reciprocal temperature between 10 and 45 °C for all spin labels, the activation energies for oxygen diffusion in the POPC and POPC−$(LA)_{12}$ membranes were evaluated from the slopes (Table 2). In the presence of 10 mol % $(LA)_{12}$, the activation energy at all positions is increased by 10−25%. The effect is strongest in the central region of the membrane.

Effects of $(LA)_{12}$ on Membrane Profiles of the Oxygen Transport Parameter. The membrane profiles of the oxygen transport parameter $W(x)$, plotted as a function of the location of the free radical, were constructed for POPC and POPC−$(LA)_{12}$ membranes [10 mol % $(LA)_{12}$] at 10, 20, 35, and 45 °C (Figure 4). The profile for the POPC−L_{24} membrane (10 mol % L_{24}) at 20 °C (*38*) is also included in Figure 4A for comparison. Large decreases in $W(x)$ across the entire lipid bilayer were induced by incorporation of $(LA)_{12}$ in the membrane. This result presents a marked contrast with the effects of L_{24} (10 mol %), which were much smaller. The difference in effects between the peptides is greatest in the central region of the membrane, where 10 mol % $(LA)_{12}$ reduced $W(x)$ by a factor of about 2, while 10 mol % L_{24} gave practically no effect. Near the membrane surface (the 5-PC position), $(LA)_{12}$ decreases $W(x)$ by 40%, while L_{24} does so by 25% (see profiles in Figure 4A). $(LA)_{12}$ also decreased the oxygen transport parameter in the polar headgroup region of POPC membranes by 25−40%. At all temperatures, membrane profiles of $W(x)$ are flattened in the presence of $(LA)_{12}$.
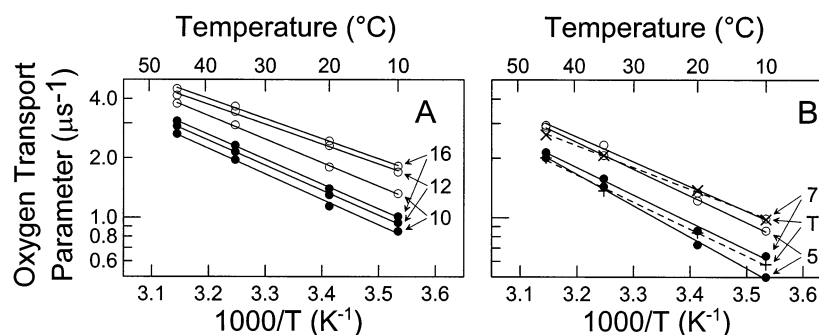
FIGURE 3: $W(x)$ plotted as a function of reciprocal temperature for spin labels in POPC (○) and POPC−(LA)$_{12}$ (10 mol %) membranes (●). To better indicate the effects of (LA)$_{12}$, data for 10-, 12-, and 16-PC are presented in (A) and for 5-, 7-, and TEMPO-PC in (B). For TEMPO-PC data (T), (- × -) indicates pure POPC and (- + -) indicates POPC−(LA)$_{12}$ (10 mol %).
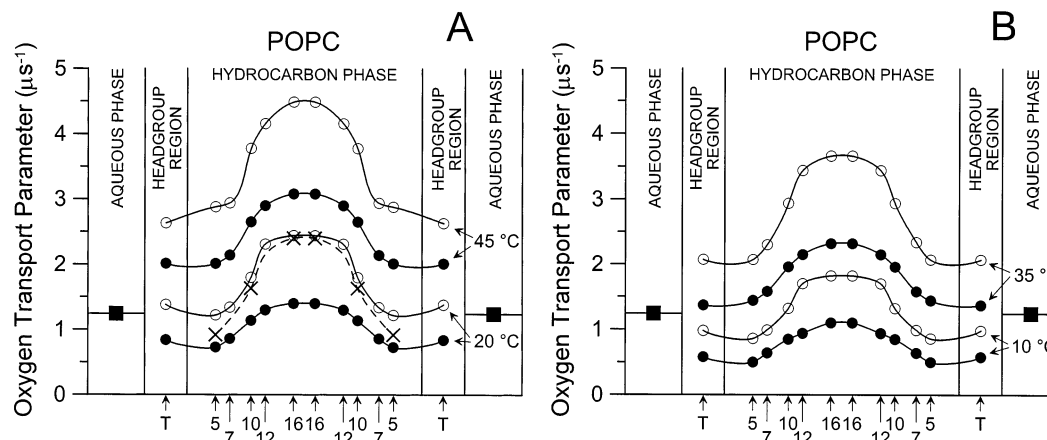

FIGURE 4: Profiles of the oxygen transport parameter $W(x)$ across the POPC bilayer in the absence (○) and presence (●) of 10 mol % (LA)$_{12}$ obtained at 45 and 20 °C (A) and at 35 and 10 °C (B). A $W(x)$ profile obtained in the presence of 10 mol % L$_{24}$ at 20 °C is also shown (- × -) (data from ref *38*).

Table 2: Activation Energy for the Translational Diffusion of Molecular Oxygen in POPC−(LA)$_{12}$ Membranes Calculated for Temperature Range 10−45 °C at Different Depths in the Membrane

(LA)$_{12}$ (mol %)	activation energy (kcal/mol)					
	T-PC	5-PC	7-PC	10-PC	12-PC	16-PC
0	5.0	6.2	5.6	5.4	4.6	4.6
10	6.3	7.1	6.2	5.8	5.7	5.7

Effects of (LA)$_{12}$ on Hydrocarbon Chain Order. The effect of (LA)$_{12}$ on the hydrocarbon chain order was studied at five depths (5-, 7-, 10-, 12-, 16-PC) in POPC membranes. Figure 5 shows a panel of conventional EPR spectra of various spin labels in POPC membranes containing 0 and 10 mol % (LA)$_{12}$ at 20 °C. The remarkable feature of these spectra is that none of them showed any indication of the presence of two components (weakly and strongly immobilized). Membranes containing L$_{24}$ also exhibited one-component EPR spectra (*38*). On the basis of these observations, it is concluded that, even at the highest peptide concentrations (1/10), the peptides are well dispersed, and the nitroxide moiety samples both the bulk and the boundary domains sufficiently well during the time determined by the anisotropy of the hyperfine interactions of the nitroxide (0.01 μs). This result is consistent with the saturation−recovery measurement in which all of the saturation−recovery curves were single-exponential curves. We are aware that proving the absence of a second component (strongly immobilized component) in conventional EPR spectra is difficult. Previously, we showed that $W(x)$ is a better probe for distinguish-

ing different membrane domains (discrimination by oxygen transport−the DOT method), when the lifetime of domains is longer than $W(x)^{-1}$ (*26, 38, 58*). As described above, $W(x)$ did not show any signs of the presence of two membrane domains.

Figure 6 shows the profiles of the order parameters, calculated according to Marsh (*64*), obtained with *n*-PC in POPC−(LA)$_{12}$ membranes at 20 °C. The alkyl chain order increases gradually with increase of the (LA)$_{12}$ concentration. As can be seen from Figure 7, the increase is largely proportional to the peptide-to-lipid ratio, which also supports our conclusion that peptide molecules are well dispersed in the POPC bilayer. The effect is greater than that caused by L$_{24}$.

Figure 8 shows the effect of (LA)$_{12}$ on the alkyl chain order displayed as a function of temperature. With a lowering of temperature, the alkyl chain order increases. The effect of 10 mol % (LA)$_{12}$ on the order parameter is similar to that of lowering the temperature by 12−18 °C, while the effect of 10 mol % L$_{24}$ is similar to that of lowering the temperature by about 8 °C (*38*). Our results differ somewhat from those presented by Pare et al. (*42*), who used ²H NMR to demonstrate that both (LA)$_{12}$ and L$_{24}$ have roughly comparable ordering effects on the liquid-crystalline state of POPC membranes. The reader, however, should be cautioned that the order parameter was calculated here using a rather simplistic method of spectral analysis. It is possible that the order parameter contains some contributions from slow motion, at least at lower temperatures. This could be the
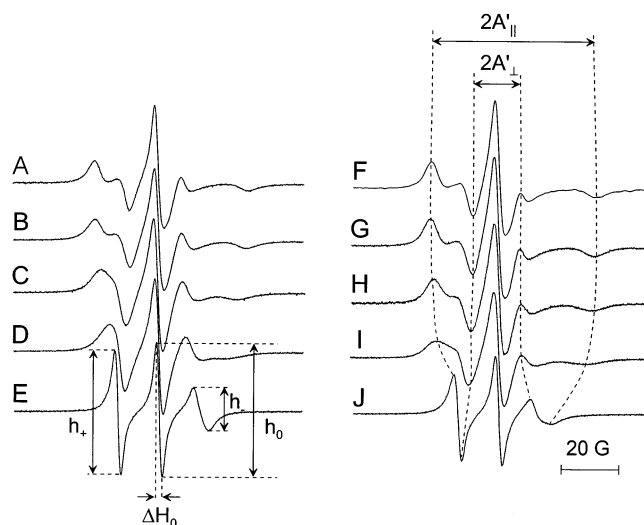
FIGURE 5: Panel of EPR spectra of 5-, 7-, 10-, 12-, and 16-PC in POPC membranes in the absence (A–E) and the presence (F–J) of 10 mol % (LA)$_{12}$ at 20 °C. Measured values for evaluating order parameters and rotational correlation times are indicated. The order parameter S was calculated according to Marsh (*64*) using the equation $S = 0.5407(A_{\parallel}' - A_{\perp}')/a_0$, where $a_0 = (A_{\parallel}' + 2A_{\perp}')/3$. The rotational correlation time was calculated according to Berliner (*66*) from the linear term of the line width parameter, $\tau_{2B} = (6.51 \times 10^{-10})\Delta H_0[(h_0/h_-)^{1/2} - (h_0/h_+)^{1/2}]s$, and with the quadratic term, $\tau_{2C} = (6.51 \times 10^{-10})\Delta H_0[(h_0/h_-)^{1/2} + (h_0/h_+)^{1/2} - 2]s$.
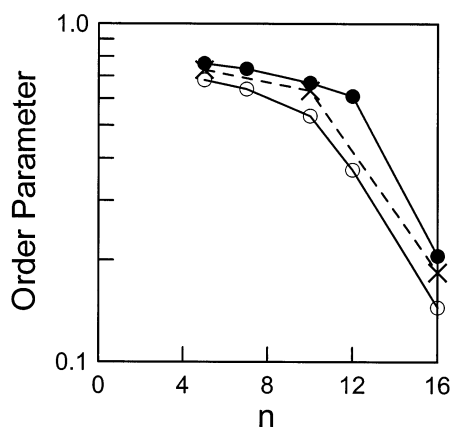

FIGURE 6: Profiles of the molecular order parameter [order parameter is plotted in a log scale as a function of nitroxide position (*n*) along the acyl chain in *n*-PC] at 20 °C obtained with 5-, 7-, 10-, 12-, and 16-PC in POPC–(LA)$_{12}$ membranes [0 and 10 mol % (LA)$_{12}$ are indicated by ○ and ●, respectively]. An order parameter profile in the presence of 10 mol % L$_{24}$ at 20 °C is also shown (- × -) (data from ref *38*).

reason for the discrepancy between the results obtained here with EPR spectroscopy and those obtained with ^{2}H NMR (*42*).

Interestingly, conventional EPR and ^{2}H NMR spectroscopic studies of (LA)-based ditryptophan-terminated WALP peptides incorporated into disaturated PC bilayers of comparable hydrophobic thickness exhibit small or no changes in hydrophobic chain orientational order, suggesting that these WALP peptides behave differently than (LA)$_{12}$ and L$_{24}$. However, single-component EPR spectra are observed, indicating that these WALP peptides, like (LA)$_{12}$ and L$_{24}$, are well dispersed even at a peptide-to-lipid ratio of 1/10, although these WALP peptides do not contain charged dilysine terminae (*65*).

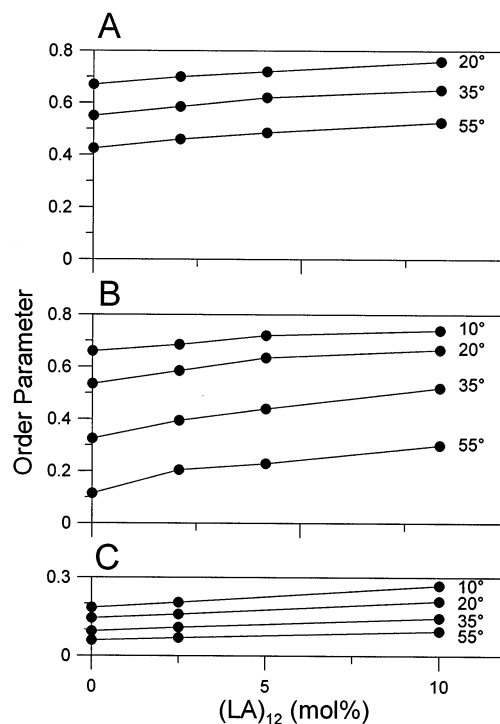
FIGURE 7: Molecular order parameters of 5- (A), 10- (B), and 16-PC (C) in POPC membranes plotted as a function of the mole fraction of (LA)$_{12}$ at 10, 20, 35,, and 55 °C.
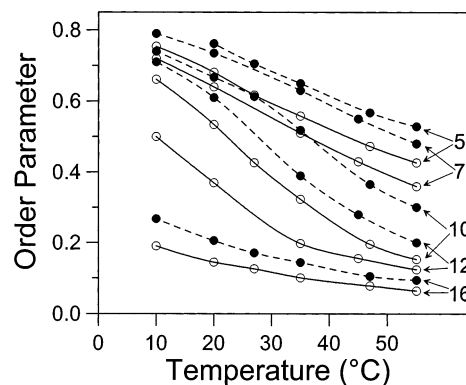

FIGURE 8: Molecular order parameters of 5-, 7-, 10-, 12-, and 16-PC in POPC (○) and POPC–(LA)$_{12}$ (10 mol %) (●) membranes, plotted as a function of temperature.

Effects of (LA)$_{12}$ on the 16-PC Reorientational Rate. The effective rotational correlation time of 16-PC was obtained by assuming isotropic rotational diffusion of the attached nitroxide (*66*). τ_{2B} was obtained from the linear term of the line width parameter, while τ_{2C} was obtained from the quadratic term (see Figure 5 for details). When τ_{2B} and τ_{2C} are similar, it is argued that the motional model is fairly good and motion is isotropic. Addition of (LA)$_{12}$ decreases the motional freedom of 16-PC at all temperatures, which is monitored by a large increase in the effective rotational correlation time (data not shown). At high temperatures (35–55 °C), calculated τ_{2B} and τ_{2C} are very similar in the absence and presence of (LA)$_{12}$, and this is an indication that (LA)$_{12}$ decreases the rate of motion but does not influence its isotropy. At lower temperatures (10–20 °C), however, the presence of (LA)$_{12}$ increases the difference between τ_{2B} and τ_{2C}, indicating the onset of anisotropic rotational diffusion. At higher temperatures, the effect of (LA)$_{12}$ is comparable
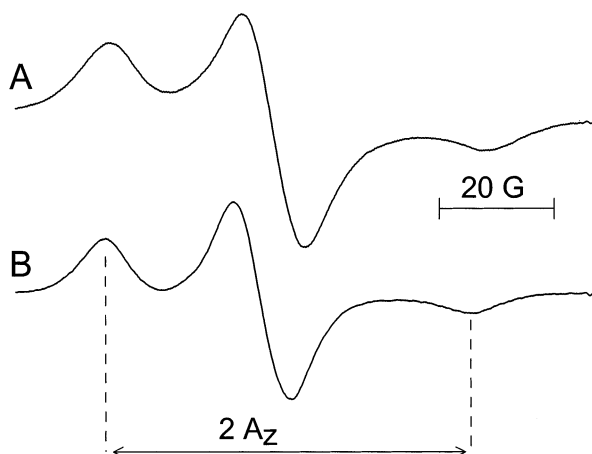
FIGURE 9: EPR spectra of 10-PC in POPC membranes in the absence (A) and presence (B) of 10 mol % $(LA)_{12}$ measured at -165 °C. The measured $2A_Z$ value (z component of the hyperfine interaction tensor) is indicated.
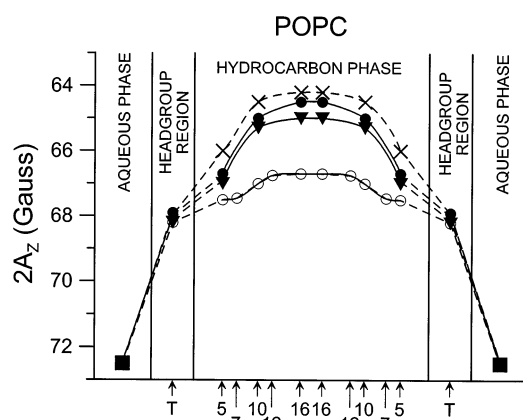

FIGURE 10: Hydrophobicity profiles ($2A_Z$) across POPC membranes containing 0, 2.5, and 10 mol % $(LA)_{12}$ (○, ▼, and ●, respectively). Data obtained with TEMPO- and *n*-PCs. Upward changes indicate increases in hydrophobicity. $2A_Z$ for 16-PC in the aqueous phase (■) was calculated from the isotropic hyperfine constant of the nitroxide spin label. Because TEMPO-PC contains a different nitroxide moiety, its points are connected with broken lines. A hydrophobicity profile obtained in the presence of 10 mol % L_{24} is also shown (- × -) (data from ref *38*).

to that of L_{24}, whereas at lower temperatures, the effect of $(LA)_{12}$ is greater than that of L_{24} (*38*).

Hydrophobicity Profiles across POPC$-(LA)_{12}$ Membranes. The effect of $(LA)_{12}$ on the hydrophobicity of the membrane interior was studied at four different depths in the POPC membrane. Figure 9 shows a conventional EPR spectra of 10-PC in POPC membranes containing 0 and 10 mol % $(LA)_{12}$ for a frozen suspension of liposomes at -165 °C. These spectra demonstrate that the effect of the peptide is primarily to change A_Z and not to reduce spin−spin interactions at the intermediate position of the nitroxide moiety on the acyl chain.

Figure 10 shows hydrophobicity profiles across POPC membranes in the presence of 2.5 and 10 mol % $(LA)_{12}$ as well as in the presence of 10 mol % L_{24} (*38*). Here, the $2A_Z$ data are presented as a function of the approximate position of the nitroxide moiety of the spin label within the lipid bilayer. The width of the hydrocarbon phase and the locations of the nitroxide moiety in the stearic acid chain are simply scaled to the number of carbon atoms in the hydrocarbon

chain. Smaller $2A_Z$ values (upward changes in the profiles) indicate higher hydrophobicity (*38, 44*).

All hydrophobicity profiles show a typical bell-like shape with a gradual increase of the hydrophobicity toward the bilayer center. $(LA)_{12}$ increases the hydrophobicity of the central part of the membrane from the level of 1-decanol ($\epsilon = 10$) to the level between hexane and dipropylamine ($\epsilon = 2-3$). We relate local hydrophobicity as observed by $2A_Z$ to hydrophobicity (or ϵ) of bulk organic solvents by referring to Figure 2 in Subczynski et al. (*44*). The effect of $(LA)_{12}$ is smaller than that of L_{24}, perhaps because the polarity of the peptide surface is higher for $(LA)_{12}$. When all leucines are replaced by alanines (A_{24}), the polarity of the peptide surface is so large that it remains in the water phase outside the membrane (*39*). The effect of both peptides, L_{24} and $(LA)_{12}$, is different from that of gramicidin A, which decreases the hydrophobicity across the PC lipid bilayers—hydrophobicity profiles become very flat (*67, 68*). Since $16-18$ phosphatidylcholine molecules surround each α-helical transmembrane peptide in gel phase membranes (*37*) in the membrane containing 10 mol % peptide, the hydrophobicity profile describes a membrane property at the peptide−lipid interface.

GENERAL DISCUSSION

The Brush-Like Surface of $(LA)_{12}$ Is Responsible for Decreasing the W(x). In the POPC lipid bilayer containing the transmembrane α-helical peptides L_{24} and $(LA)_{12}$, the exchange rate of lipids between all domains in the membrane must be greater than 6×10^6 s^{-1} because the peptide-rich membranes appear as homogeneous membranes for conventional and saturation−recovery EPR. Since about $10-12$ molecules of phospholipid are required to surround a transmembrane α-helical peptide in fluid phase PC bilayers, these peptides must form peptide-rich regions at 10 mol %, at least transiently.

Our results suggest that the lipid exchange rates among the bulk, boundary, and peptide-rich regions are fast and/or that the peptide-rich domains must be forming and dispersing rapidly (*38*; present work). This means that the striking difference between the effect of L_{24} and $(LA)_{12}$ on oxygen transport within the POPC membrane is not a result of the different packing of these peptides in the lipid bilayer. This difference is believed to be a consequence of differing organization of the L_{24} and the $(LA)_{12}$ hydrophobic surfaces as well as differing interactions of peptide side chains with the lipid hydrocarbon chains. In L_{24}, all amino acids that form the hydrophobic α-helical core of the peptide are leucines, and their isobutyl side chains are packed tightly, giving a rather hard, smooth, hydrophobic surface. In $(LA)_{12}$, half of the amino acids are replaced by alanine residues, and these amino acids are placed alternately with leucine residues in the transmembrane α-helical segment. Alternately positioned small methyl side groups of alanines and the large isobutyl side chains of leucines result not only in significant roughness of the hydrophobic surface of $(LA)_{12}$ but also in significant freedom of motion of the isobutyl side chains of leucines (flexible brush-like surface). With this new organization of the hydrophobic surface, the isobutyl side chains of $(LA)_{12}$ can protrude between the hydrocarbon chains of lipid molecules. Flexibility of both side chains of the peptide and hydrocarbon chains of lipids allows for better mixing

and stronger interaction of these two components. In this model, both the frequency of *gauche–trans* isomerization of hydrocarbon chains and the concentration of vacant pockets (voids) in the lipid bilayer are reduced, which decreases oxygen transport.

Comparison of the effects of L_{24} and $(LA)_{12}$ on oxygen transport parameter and hydrophobicity profiles gives additional insight into the mechanism of the interactions of these peptides with the POPC bilayer. In lipid bilayer membranes, the overall shape of the hydrophobicity profile is similar to the shape of the oxygen transport parameter profile. Both are bell-shaped, with a maximum at the membrane center and somewhat similar values in the polar headgroup and hydrocarbon near-polar headgroup regions. This correspondence is expected because a higher hydrophobicity should produce better solubility of hydrophobic solutes such as oxygen.

An understanding of the nature of the EPR measurements involved in obtaining these profiles will help to perform more detailed analysis. The hydrophobicity profile measured by the spin labeling method is largely determined by the extent of water penetration into the membrane, since dehydration abolishes the hydrophobic gradient in liposome samples (*69*). This profile can thus be related to the distribution of polar as well as nonpolar molecules across the lipid bilayer. Oxygen transport parameter profiles are obtained by measurement of the collision rate between molecular oxygen and the free radical moiety of the lipid spin label (*43*, *48*, *50*) and depend on both local solubility and the local translational diffusion coefficient of oxygen in membranes.

With this in mind, one can compare the effects of different membrane modifiers in PC membranes. For example, the effect of cholesterol on both profiles is similar: cholesterol increases hydrophobicity and the oxygen transport parameter in the membrane center and decreases them in the polar headgroup region and hydrocarbon region near the membrane surface (*44*, *50*, *70*, *71*). It can thus be assumed that solubility (distribution of oxygen molecules within the lipid bilayer) makes a significant contribution to the changes in the oxygen transport parameter profile. The effect of $(LA)_{12}$ on both profiles is different. This peptide increases hydrophobicity across the POPC bilayer and at the same time decreases the oxygen transport parameter across the entire membrane. In both cases, the effect is strongest in the membrane center. This suggests that the major effect of $(LA)_{12}$ is to decrease the oxygen translational diffusion within the PC bilayer. In addition, the activation energy for translational diffusion of molecular oxygen, which describes the barrier for oxygen transport in the POPC bilayer, is increased. L_{24}, which increases membrane hydrophobicity more than $(LA)_{12}$, has practically no effect on the oxygen transport (*38*). Our model is that the flexible brush-like surface of $(LA)_{12}$ reduces the appearance and movement of vacant pockets (voids) in the vicinity close to the peptide, which are the carriers for oxygen molecules. The hard, smooth surface peptide, L_{24}, affects the membrane organization and dynamics observed by conventional EPR (order and motion of lipid hydrocarbon chains) in a manner somewhat similar to $(LA)_{12}$, but not transport of molecular oxygen. Molecular oxygen appears again to be a very useful probe for investigation of membrane dynamics.
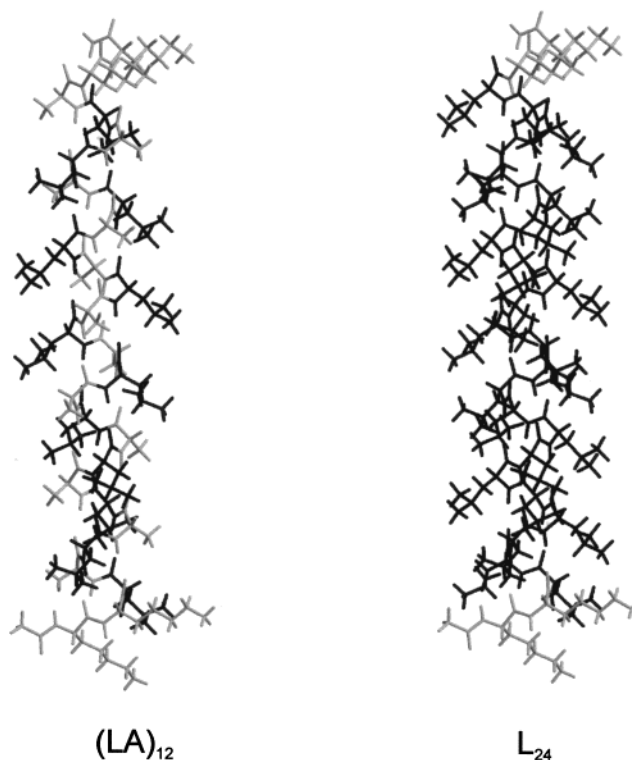

$(LA)_{12}$ $\qquad$ L_{24}

FIGURE 11: Three-dimensional structures of $(LA)_{12}$ and L_{24} after 1000 ps simulation time. Leucine residues are shown as black lines and alanine and lysine as gray lines. The image was produced with MolScript (*75*) and Raster3D (*76*).

Molecular Dynamics Simulations Confirm Our Model. As there are 3.6 residues per turn in an α-helix and the rise per residue is 1.5 Å, the neighboring residues are 100° apart, and the vertical separation between the n and $n + 4$ residues is 6 Å. Thus, the vertical separation between leucine side chains in both L_{24} and $(LA)_{12}$ is the same, whereas the angular separation between two neighboring leucine side chains is two times larger in $(LA)_{12}$ than in L_{24} (200° and 100°, respectively). In both peptides, leucine side chains have space for rotation. However, since two pairs of leucine side chains in $(LA)_{12}$ are separated by a short side chain of alanine, the rotational freedom of the leucine side chains is expected to be larger. Indeed, the average, over all residues in the peptide and four time frames of the S_{mol} parameter, is 0.35 ± 0.09 for $(LA)_{12}$ and 0.47 ± 0.07 for L_{24}.

Because the side chain of alanine is much shorter than that of leucine, alanine residues in $(LA)_{12}$ create two spiral grooves on the peptide surface. This might facilitate interpenetration of PC hydrocarbon chains and leucine side chains. The gaps between side chains in L_{24} are too narrow to allow for interpenetration of PC hydrocarbon chains and leucine side chains. This can be seen in Figure 11, in which configurations of both $(LA)_{12}$ and L_{24} are shown after 1000 ps MD simulation. The display indicates a loose packing of the leucine side chains in $(LA)_{12}$ and much denser packing in L_{24}.

Significance for Site-Directed Spin Labeling. As was mentioned by Marsh (*71*), both hydrophobicity and oxygen transport parameter profiles have significant practical applications in site-directed spin labeling for depth determination. In that method, spin labels are covalently attached to the protein and sense the protein interior or the protein–

lipid interface. Accessibility studies with complementary relaxation agents (hydrophobic oxygen molecules and the polar paramagnetic metal complexes) are most informative, especially for depth determination of the lipid-exposed sites in a membrane. In these measurements, a free radical fragment of the spin label attached covalently to the protein senses only the membrane environment in the immediate vicinity of the protein surface (*72*). The results presented earlier (*38*) and in this paper suggest that the transmembrane α-helical peptides affect the local hydrophobicity as well as the local mobility of small molecules such as oxygen, and these effects are strongly dependent on the amino acid composition of the peptide (*67*, *68*). Because these results were obtained with lipid spin labels at high peptide concentration, they contain information about the membrane environment close to the peptide surface. This is also the environment sensed by spin labels covalently attached to proteins in the site-directed spin labeling approach. To obtain depth measurements, calibration of the accessibility of different relaxation agents (accessibility profiles) into the lipid bilayer is performed using *n*-PC spin labels (*73*). These profiles not only depend on the lipid composition of the host membrane (*74*) but also are affected, as we show here, by the transmembrane peptides and integral membrane proteins (*58*).

ACKNOWLEDGMENT

REFERENCES

1. Edidin, M. (1990) *Curr. Top. Membr. Trans. 36*, 81−93.
2. Edidin, M. (1997) *Curr. Opin. Struct. Biol. 7*, 528−532.
3. Edidin, M., and Stroyanovski, I. (1991) *J. Cell Biol. 112*, 1145−1150.
4. Kusumi, A., and Sako, Y.(1996) *Curr. Opin. Cell Biol. 8*, 566−574.
5. Simons, K., and Ikonen, E. (1997) *Nature 387*, 569−572.
6. Mouritsen, O. G., and Andersen, O. S. (1998) *Biol. Skr.−K. Dan. Vidensk. Selsk. 49*.
7. Brown, D. A. (2001) *Proc. Natl. Acad. Sci. U.S.A. 98*, 10517−10518.
8. Schroeder, F., Gallegos, A. M., Atshaves, B. P., Storey, S. M., McIntosh, A. L., Petrescu, A. D., Huang, H., Starodub, O., Chao, H., Yang, H., Frolov, A., and Kier, A. B. (2001) *Exp. Biol. Med. 226*, 873−890.
9. Jacobson, K., and Dietrich, C. (1999) *Trends Cell. Biol. 9*, 87−91.
10. Simons, K., and Toomre, D. (2000) *Nat. Rev. Mol. Cell Biol. 1*, 31−39.
11. Ikonen, E. (2001) *Curr. Opin. Cell Biol. 13*, 534−542.
12. Galbiati, F., Razani, B., and Lisanti, M. P. (2001) *Cell 106*, 403−411.
13. Dykstra, M. L., Cherukuri, A., and Pierce, S. K. (2001) *Traffic 2*, 160−166.
14. Viola, A. (2001) *Trends Immunol. 22*, 322−327.
15. van Meer, G. (2002) *Science 296*, 855−857.
16. Hakomori, S. (2002) *Proc. Natl. Acad. Sci. U.S.A. 99*, 225−232.
17. Adams, C., and Nelson, W. J. (1998) *Curr. Opin. Cell Biol. 7*, 457−463.
18. Kusumi, A., Suzuki, K., and Koyasako, K. (1999) *Curr. Opin. Cell Biol. 11*, 582−590.
19. Iino, R., Koyama, I., and Kusumi, A. (2001) *Biophys. J. 80*, 2667−2776.
20. Smart, E. J., Graf, G. A., McNiven, M. A., Sessa, W. C., Engelman, J. A., Scherer, O. E., Okamoto, T., and Lisanti, M. P. (1999) *Mol. Cell. Biol. 19*, 7289−7304.
21. Kurzchalia, T. V., and Patron, R. G. (1999) *Curr. Opin. Cell Biol. 11*, 424−431.

22. Simons, K., and Ehehalt, R. (2002) *J. Clin. Invest. 110*, 597−603.
23. Subczynski, W. K., Antholine, W. E., Hyde, J. S., and Kusumi, A. (1990) *Biochemistry 29*, 7936−7945.
24. Pasenkiewicz-Gierula, M., Subczynski, W. K., and Kusumi, A. (1991) *Biochimie 73*, 1311−1316.
25. Gaidarov, I., Santini, F., Warren, R. A., and Keen, J. H. (1999) *Nat. Cell Biol. 1*, 1−7.
26. Kawasaki, K., Yin, J.-J., Subczynski, W. K., Hyde, J. S., and Kusumi, A. (2001) *Biophys. J. 80*, 738−748.
27. White, S. H., and Wimley, W. C. (1998) *Biochim. Biophys. Acta 1376*, 339−352.
28. Killian, J. A. (1998) *Biochim. Biophys. Acta 1376*, 401−416.
29. Davis, J. M., Clare, J. M., Hodges, R. S., and Bloom, M. (1983) *Biochemistry 22*, 5298−5305.
30. Zhang, Y.-P., Lewis, R. N. A. H., Hodges, R. S., and McElhaney, R. N. (1992) *Biochemistry 31*, 11572−11578.
31. Zhang, Y.-P., Lewis, R. N. A. H., Hodges, R. S., and McElhaney, R. N. (1992) *Biochemistry 31*, 11579−11588.
32. Axelsen, P. H., Kaufman, P. H., McElhaney, R. N., and Lewis, R. N. A. H. (1995) *Biophys. J. 69*, 2770−2781.
33. Huschilt, J. C., Millman, B. M., and Davis, J. H. (1989) *Biochim. Biophys. Acta 979*, 139−141.
34. Bolen, E. J., and Holloway, P. W. (1990) *Biochemistry 29*, 9638−9643.
35. Zhang, Y.-P., Lewis, R. N. A. H., Hodges, R. S., and McElhaney, R. N. (1995) *Biophys. J. 68*, 847−857.
36. Huschilt, J. C., Hodges, R. S., and Davis, J. H. (1985) *Biochemistry 24*, 1377−1386.
37. Morrow, M. R., Huschilt, J. C., and Davis, J. H. (1985) *Biochemistry 24*, 5396−5406.
38. Subczynski, W. K., Lewis, R. N. A. H., McElhaney, R. N., Hodges, R. S., Hyde, J. S., and Kusumi, A. (1998) *Biochemistry 37*, 3156−3164.
39. Lewis, R. N. A. H., Zhang, Y.-P., Hodges, R. S., Subczynski, W. K., Kusumi, A., Flach, C. R., Mendelsohn, R., and McElhaney, R. N. (2001) *Biochemistry 40*, 12103−12111.
40. Zhang, Y.-P., Lewis, R. N. A. H., Henry, G. D., Sykes, B. D., Hodges, R. S., and McElhaney, R. N. (1995) *Biochemistry 34*, 2348−2361.
41. Zhang, Y.-P., Lewis, R. N. A. H., Hodges, R. S., and McElhaney, R. N. (1995) *Biochemistry 34*, 2362−2371.
42. Pare, Ch., Laflear, M., Liu, F., Lewis, R. N. A. H., and McElhaney, R. N. (2001) *Biochim. Biophys. Acta 1511*, 60−73.
43. Kusumi, A., Subczynski, W. K., and Hyde, J. S. (1982) *Proc. Natl. Acad. Sci. U.S.A. 79*, 1854−1858.
44. Subczynski, W. K., Wisniewska, A., Yin, J.-J., Hyde, J. S., and Kusumi, A. (1994) *Biochemistry 33*, 7670−7681.
45. Yin, J.-J., and Hyde, J. S. (1987) *Z. Phys. Chem. (Munich) 153*, 57−65.
46. Yin, J.-J., Feix, J. B., and Hyde, J. S. (1990) *Biophys. J. 58*, 715−720.
47. Yin, J.-J., and Subczynski, W. K. (1996) *Biophys. J. 71*, 832−839.
48. Subczynski, W. K., Hyde, J. S., and Kusumi, A. (1989) *Proc. Natl. Acad. Sci. U.S.A. 86*, 4474−4478.
49. Hyde, J. S., and Subczynski, W. K. (1989) in *Biological Magnetic Resonance, Vol. 8. Spin Labeling: Theory and Applications* (Berliner, L. J., and Reuben, J., Eds.) pp 399−425, Plenum Press, New York.
50. Subczynski, W. K., Hyde, J. S., and Kusumi, A. (1991) *Biochemistry 30*, 8578−8590.
51. Fischkoff, S., and Vanderkooi, J. M. (1975) *J. Gen. Physiol. 65*, 663−676.
52. Subczynski, W. K., and Hyde, J. S. (1981) *Biochim. Biophys. Acta 643*, 283−291.
53. Hyde, J. S., and Subczynski, W. K. (1984) *J. Magn. Reson. 56*, 125−130.
54. Subczynski, W. K., and Hyde, J. S. (1984) *Biophys. J. 45*, 743−748.
55. Pearlman, D. A., Case, D. A., Caldwell, J. C., Seibel, G. L., Singh, U. C., Weiner, P. K., and Kollman, P. A. (1991) AMBER 4.0, University of California, San Francisco.
56. Case, D. A., Pearlman, D. A., Caldwell, J. W. M., Cheatham, T. E., III, Ross, W. S., Simmerling, Ch., Darden, T. A., Merz, K. M., Stanton, R. V., Cheng, A. L., Vincent, J. J., Crowley, M., Ferguson, D. M., Radmer, R. J., Seibel, G. L., Singh, U. C., Weiner, P. K., and Kollman, P. A. (1997) AMBER 5.0, University of California, San Francisco.

57. Hubbell, W. L., and McConnell, H. M. (1971) *J. Am. Chem. Soc. 93*, 314−326.

58. Ashikawa, I., Yin, J.-J., Subczynski, W. K., Kouyama, T., Hyde, J. S., and Kusumi, A. (1994) *Biochemistry 33*, 4947−4952.

59. Atkins, P. W., and Kivelson, D. (1966) *J. Chem. Phys. 44*, 169−174.

60. Bloemberg, N., Purcell, E. M., and Pound, R. V. (1943) *Phys. Rev. 73*, 679−712.

61. McConnell, H. M. (1956) *J. Chem. Phys. 25*, 709−711.

62. Subczynski, W. K., and Hyde, J. S. (1983) *Biophys. J. 41*, 283−286.

63. Smotkin, E. S., Moy, F. T., and Plachy, W. Z. (1991) *Biochim. Biophys. Acta 1061*, 33−38.

64. Marsh, D. (1981) in *Membrane Spectroscopy* (Grell, E., Ed.) pp 51−142, Springer-Verlag, Berlin.

65. de Planque, M. R. R., Greathouse, D. V., Koeppe, R. E., Schafer, H., Marsh, D., and Killian, J. A. (1998) *Biochemistry 37*, 9333−9345.

66. Berliner, L. J. (1978) *Methods Enzymol. 49*, 466−470.

67. Ge, M., and Freed, J. H. (1993) *Biophys. J. 65*, 2106−2123.

68. Wisniewska, A., and Subczynski, W. K. (1996) *Curr. Top. Biophys. 20*, 86−92.

69. Griffith, O. H., Dehlinger, P. J., and Van, S. P. (1974) *J. Membr. Biol. 15*, 159−192.

70. Marsh, D., and Watts, A. (1981) in *Liposomes: from Physical Structure to Therapeutic Applications* (Knight, C. G., Ed.) pp 139−188, Elsevier/North-Holland Biomedical Press, Amsterdam.

71. Marsh, D. (2001) *Proc. Natl. Acad. Sci. U.S.A. 98*, 7777−7782.

72. Feix, J. B., and Klug, C. S. (1998) in *Biological Magnetic Resonance, Vol. 14. Spin Labeling: The Next Millennium* (Berliner, L. J., Ed.) pp 251−281, Plenum Press, New York.

73. Altenbach, C., Greenhalgh, D. A., Khorana, H. G., and Hubbell, W. L. (1994) *Proc. Natl. Acad. Sci. U.S.A. 91*, 1667−1671.

74. Farahbakhsh, Z. T., Altenbach, C., and Hubbell, W. L. (1992) *Photochem. Photobiol. 56*, 1019−1033.

75. Kraulis, P. (1991) *J. Appl. Crystallogr. 24*, 9446−9450.

76. Merritt, E. A., and Bacon, D. J. (1997) *Methods Enzymol. 277*, 505−524.